Angewandte Chemie
Eine Zeitschrift der Gesellschaft Deutscher Chemiker

Supporting Information

Charge Neutralization Drives the Shape Reconfiguration of DNA Nanotubes

Pi Liu[+], Yan Zhao[+], Xiaoguo Liu[+], Jixue Sun[+], Dede Xu, Yang Li, Qian Li, Lihua Wang, Sichun Yang, Chunhai Fan, and Jianping Lin**

anie_201801498_sm_miscellaneous_information.pdf

Supporting information

Table of Contents:

Tables

Table S1. Stretch modulus and persistence length of centre 42 bp in five systems

System	Stretch modulus (PN)	Persistence length (nm)	Length (nm)	Radius (nm)
250 mM Na^+	4208.44 ± 111.23	392.74 ± 10.00	12.47	6.75
500 mM Na^+	3779.34 ± 104.62	385.27 ± 9.31	12.57	6.11
500 mM Na^+_E6HB	4830.59 ± 171.04	400.55 ± 9.00	12.41	6.11
125 mM Mg^{2+}	4159.40 ± 141.44	464.55 ± 17.89	12.69	5.38
250 mM Mg^{2+}	4779.96 ± 80.47	388.94 ± 9.04	12.51	5.08

Table S2. Calculated FRET efficiency and Cy3-Cy5 pair distance of 6HB-DNA under different buffer conditions

Sample	FRET efficiency*	Cy3-Cy5 pair distance (nm)
125.0 mM $MgCl_2$	0.578	5.21
50.0 mM $MgCl_2$	0.550	5.32
12.5 mM $MgCl_2$	0.472	5.60
100.0 mM NaCl	0.273	6.49

*(See experimental part of supporting information for detailed FRET efficiency calculation method)

Table S3. Comparison of the Radius of Gyration (Rg) for 6HB-DNA Derived from Experimental and Theoretical (CRYSOL) Scattering Profiles

Sample	Rg (nm) Experimental	Rg (nm) Theoretical*
125.0 mM $MgCl_2$	7.5 + 0.1	7.7
50.0 mM $MgCl_2$	7.5 + 0.2	7.7
12.5 mM $MgCl_2$	7.9 + 0.1	-
100.0 mM NaCl	8.7 + 0.1	8.4
blank	8.0 + 0.3	8.1
C_2H_5	7.8 + 0.2	7.9

*Values were determined from Guinier fits of the scattering profiles generated from corresponding fitting PDB files in the range qmax•Rg < 1.3.

Experimental

1. Materials

DNA oligonucleotides were purchased from JIE LI Biology (Shanghai), and phosphorothioate-modified DNA (PPT-DNA) oligonucleotides were purchased from Sangon Biotech (Shanghai) Co., Ltd. using High Performance Liquid Chromatography (HPLC) purification. Iodo-ethane was purchased from Sigma Aldrich. The other reagents were purchased from Sinopharm Chemical Reagent Co., Ltd. All chemicals were used without further purification.

2. Methods

2.1 Assembly of 6-helix bundle (6HB) DNA

Sixteen strands of equimolar amounts of DNA oligonucleotides (1 μM) were mixed in specified buffer with different ion strength (total volume 100 μL), then slowly cooled down from 95 °C to room temperature in water bath for 12 hours (in a 1L Styrofoam box). Buffers: 6HB-12.5 mM Mg^{2+} buffer (40 mM Tris, 20 mM acetic acid, 2 mM EDTA and 12.5 mM magnesium acetate, pH 8.0), 6HB-50 mM Mg^{2+} buffer (40 mM Tris, 20 mM acetic acid, 2 mM EDTA, and 50 mM magnesium acetate, pH 8.0) , 6HB-125 mM Mg^{2+} buffer (40 mM Tris, 20 mM acetic acid, 2 mM EDTA, and 125 mM magnesium acetate, pH 8.0) and 6HB-Na^{+} buffer (40 mM Tris, 20 mM acetic acid, 2 mM EDTA, and 100 mM sodium acetate, pH 8.0).

2.2 Ethylation of phosphorothioate-DNA

Ethylation modification of PPT-DNA oligonucleotides referred to a protocol proposed by Gut and Beck[1]. 1 μL PPT-DNA oligonucleotides (1 mM) were dissolved in 5 μL DMF-Tris buffer which contained 90% N, N-dimethylformamide (DMF) and 10% Tris-HCl (pH 8.0). 20 equivalents per PPT group of iodo-ethane were then added, and the mixture in a low attachment Eppendorf tube was incubated at 65 °C for 1.5 hours. After that, the solvent was removed under reduced pressure. The obtained sample powder was dissolved in Q water (18 MΩ·cm) and purified by NAP-25 columns (GE Healthcare) to remove excess iodo-ethane. The recyclable ethylation DNA oligonucleotides were conducted mass spectrometric analysis to confirm the modifications were completed as expected.

2.3 Non-Denaturing Gel Electrophoresis

The products were run on native 6% polyacrylamide (PAGE) gel to confirm the formation of 6HB in step 2.1 and 2.2. The electrophoresis was carried out on a Bio-Rad gel electrophoresis under 100

V for 2 hours, after that, the sample were strained by gel red (Biotium, USA). A DL2000 marker was used as reference.

2.4 Fluorescence spectrum

The 6HB labelled by Cy3-Cy5 fluorescence pairs were characterized on a fluorescence spectrophotometer (Hitachi F-4500) to record fluorescence spectrum, for the current sample, excitation peak at 530 nm, emission peaks at 550 and 750 nm respectively.

We calculated the FRET efficiency and Cy3-Cy5 pair distance based on the following functions[2]:

$$E = 1 - \frac{ID_A}{ID}$$

$$E = \frac{1}{1+\left(\frac{d}{r}\right)^6}$$

Where *E* is the FRET efficiency, ID_A and *ID* are the fluorescence intensities with and without receptor, *d* is the Cy3-Cy5 pair distance and *r* = 5.5 nm is the FRET radius constant of Cy3-Cy5

2.5 Small-angle X-ray scattering (SAXS)

Small-angle X-ray scattering (SAXS) experiments were performed on beamline BL19U2 of the National Center for Protein Science Shanghai (NCPSS) at Shanghai Synchrotron Radiation Facility (SSRF). The wavelength (λ) of the X-radiation was set at 1.033 Å. Scattered X-ray intensities were measured by a Pilatus 1 M detector (DECTRIS Ltd). The sample-to-detector distance was 2125.0 mm for the current measurements, it was set such that the detecting range of momentum transfer q ($q = 4\pi\sin\theta/\lambda$, where 2θ is the scattering angle) of the SAXS experiments was 0.01 – 0.5 $Å^{-1}$ which corresponds to an investigated length scale from 10 to 600 Å. The solution temperature was held constant at room temperature, 25 °C.

Ion varieties and concentration sample group. A flow cell comprising a cylindrical quartz capillary with a diameter of 1.5 mm and a wall thickness of 10 µm was used, and the exposure time was set at 1s. The X-ray beam, with a size of 0.40 × 0.15 (H × V) mm^2, was adjusted to pass through the centers of the capillaries for each measurements. The volume of each sample was 100 µL, with 6HB-DNA concentration of 2 µM. To obtain optimized signal-to-noise ratios, 20 frames were recorded for each sample and buffer.

Ethylized sample group. Due to the low productivity of ethylized 6HB-DNA, an online HPLC system was used to get enough signal-to-noise SAXS profiles. The solution flow was controlled by

an Agilent high-performance liquid chromatography (HPLC) system configured so that samples passed sequentially through the size exclusion chromatography (SEC) column, a UV-Vis cell to measure DNA concentration (via UV absorbance at 260 nm), a multi-angle light scattering detector (DAWN HELEOS-II) and the SAXS flow cell. Data were collected using SEC-4000 (Phenomenex, USA) columns, the column were pre-equilibrated over night with 25 mM Tris-HCl (pH 7.4), 450 mM NaCl solution at a flow rate of 100 μL/min. The flow rate was then set to 500 μL/min, and 500 μL of sample solution was injected onto the column. A total of 500 SAXS images were collected during the elution, with a frame duration of 1.5 s and dead time of 0.5 s. Out of which, 20 frames were selected during the dilution peak of 6HB-DNA monomer, and 20 frames corresponding to the NaCl-Tris elution buffer were averaged to provide subtraction buffer signal.

The 2-D scattering images were converted to 1-D SAXS curves through azimuthal averaging after solid angle correction and then normalizing to the intensity of transmitted X-ray beam using the software package BioXTAS RAW 1.2.1.[3] The data were further analyzed by ATASAS 2.7.2 package and Fast-SAXS-Pro.[4]

2.6 Building protocol of DNA nanotube

The sequence and structure of the six-helix bundle DNA nanotube (6HB) in our work was derived from the work of Seeman et al.[5], with removing some base pairs that work as sticky ends to connect other nanotubes. The sequence arrangement of the 6HB are shown in **Fig. S1**, which was modified from ref 1. The sequences of six helices were presented in **Table S4**. To build the 6HB, six separate helices are aligning in a hexagonal pattern (**Fig. S2**) and the chains should be broken and reconnected at the crossovers. The inner diameter of 6HB was selected by the minimized total energy. The relationship between the total energy and inner diameter is presented in **Table S7.**

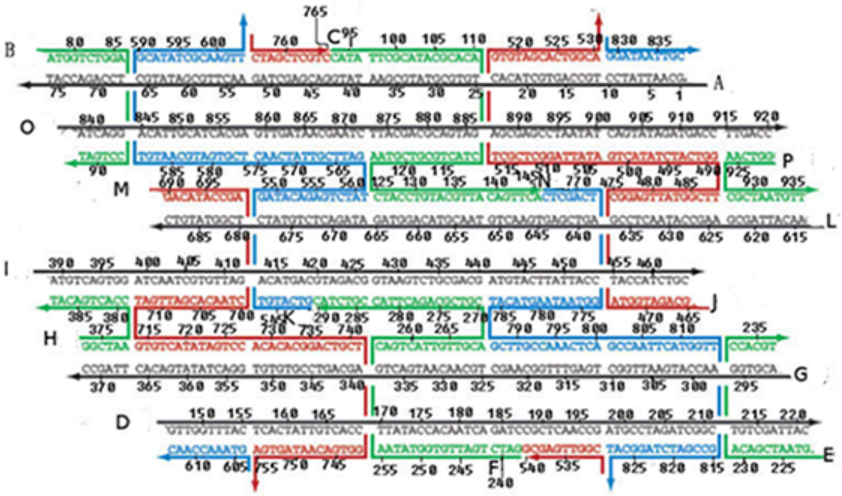

Figure S1. Schematic drawings of the six-helix bundle motif, which is modified from ref 1 with removing the sticky ends

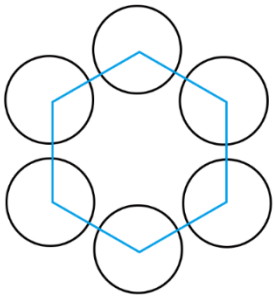

Figure S2. The DNA nanotube was constructed by aligning six separated bundles in a hexagonal pattern

Table S4. The sequences of sixteen reformed chains

A	GCAATTATCCTGCCAGTGCTACACTGTGCGTATGCGAATATGGACGAGCTAGAACTTGCGATATGCTCCAGACCAT
B	ATGGTCTGGACCTGAT
C	CATATTCGCATACGCACACTACTGCGTCGTAACTACCTGTACGTTACAGTTCA
D	GTTGGTTTACTCACTATTGTCACCTTATACCACAATCAGATCCGCTCAACCGATGCCTAGATCGGCTGTCGATTAC
E	GTAATCGACACCACGT
F	GATCTGATTGTGGTATAACAGTCATTGTTGCACGTCGCAGACTTACCGTCTAC
G	ACGTGGAACCATGAATTGGCTGAGTTTGGCAAGCTGCAACAATGACTGAGCAGTCCGTGTGTGGACTATATGACACTTAGCC
H	GGCTAACCACTGACAT
I	ATGTCAGTGGATCAATCGTGTTAGACATGACGTAGACGGTAAGTCTGCGACGATGTACTTATTACCTACCATCTGC
J	GCAGATGGTACGGAGTTATGGCTTGGTCATCTATACTGATATTAGGCTCGCTGTGTAGCACTGGCACGGTTGAGCG
K	GTCATGTGATACAGAGTCTATGATTCGTTATCAACTCGTGATGCAATGTGCATATCGCAAGTTGTAAACCAAC
L	AACATTAGCGAAGCCATAACTCCGAGTCGAGTGAACTGTAACGTACAGGTAGATAGACTCTGTATCTCGGTATGTC
M	GACATACCGACTAACACGATTGATGTGTCATATAGTCCACACACGGACTGCTGGTGACAATAGTGACTAGCTCGTC
N	CTCGACTGGTAATAAGTACATGCTTGCCAAACTCAGCCAATTCATGGTTGCCGATCTAGGCATGGATAATTGC
O	ATCAGGACATTGCATCACGAGTTGATAACGAATCTTACGACGCAGTAGAGCGAGCCTAATATCAGTATAGATGACCTTGACC
P	GGTCAACGCTAATGTT
C-Cy5	Cy5-CATATTCGCATACGCACACTACTGCGTCGTAACTACCTGTACGTTACAGTTCA
I-Cy3	ATGTCAGTGGATCAATCGTGTTAGACATGACGTA(Cy3)GACGGTAAGTCTGCGACGATGTACTTATTACCTACCATCTGC

Table S5. The sequences of sixteen reformed chains with phosphorothioate modified nucleic acids and fluorescence probe

A-PPT	GCAATTATCCTGCCAGTGCTACACTGTGCGTATGCGAATATGGACGAGCTAGAACTTGCGATA TGCTCCAGACCAT
B	ATGGTCTGGACCTGAT
C-PPT	CATATTCGCATACGCACACTACTGCGTCGTAACTACCTGTACGTTACAGTTCA
D-PPT	GTTGGTTTACTCACTATTGTCACCTTATACCACAATCAGATCCGCTCAACCGATGCCTAGATCG GCTGTCGATTAC
E	GTAATCGACACCACGT
F-PPT	GATCTGATTGTGGTATAACAGTCATTGTTGCACGTCGCAGACTTACCGTCTAC
G-PPT	ACGTGGAACCATGAATTGGCTGAGTTTGGCAAGCTGCAACAATGACTGAGCAGTCCGTGTGT GGACTATATGACACTTAGCC
H	GGCTAACCACTGACAT
I-PPT	ATGTCAGTGGATCAATCGTGTTAGACATGACGTAGACGGTAAGTCTGCGACGATGTACTTATT ACCTACCATCTGC
J	GCAGATGGTACGGAGTTATGGCTTGGTCATCTATACTGATATTAGGCTCGCTGTGTAGCACTG GCACGGTTGAGCG
K	GTCATGTGATACAGAGTCTATGATTCGTTATCAACTCGTGATGCAATGTGCATATCGCAAGTTG TAAACCAAC
L-PPT	AACATTAGCGAAGCCATAACTCCGAGTCGAGTGAACTGTAACGTACAGGTAGATAGACTCTGT ATCTCGGTATGTC
M	GACATACCGACTAACACGATTGATGTGTCATATAGTCCACACACGGACTGCTGGTGACAATAG TGACTAGCTCGTC
N	CTCGACTGGTAATAAGTACATGCTTGCCAAACTCAGCCAATTCATGGTTGCCGATCTAGGCAT GGATAATTGC
O-PPT	ATCAGGACATTGCATCACGAGTTGATAACGAATCTTACGACGCAGTAGAGCGAGCCTAATATC AGTATAGATGACCTTGACC
P	GGTCAACGCTAATGTT
C-PPT-Cy5[a]	**Cy5-**CATATTCGCATACGCACACTACTGCGTCGTAACTACCTGTACGTTACAGTTCA
I-PPT-Cy3[a]	ATGTCAGTGGATCAATCGTGTTAGACATGACGTA**(Cy3)**GACGGTAAGTCTGCGACGATGTACT TATTACCTACCATCTGC

Resname colored red represent Phosphorothioate-modified nucleic acids

[a]Cy5(Green) and Cy3(blue) represent fluorescence probe

Force field construction of ethyl-phosphorothioate nucleic acid

The charge distribution of the ethyl-phosphorothioate DNA should be generated to construct a non-standard ethyl-phosphorothioate nucleic acid residue (DSX, X = A, T, C, G). Aminomethyl group (NME) and acetyl group (ACE) as cap groups with known charges[6] (**Fig. S3A**) were added in 5' and 3' direction to build a complete molecule, respectively. A detailed capped ethyl-phosphorothioate nucleotide is shown in Fig. S3B. The charges on the base and C1' and H1' atom of sugar were used from parmbsc0 force field[7] directly. The charges on the phosphorothioate, ethyl and sugar (except C1' and H1' atom) were generated by Restrained Electrostatic Potential (RESP) method[8]. The results of charge distribution were shown in **Table S7**. The atom type OS is the same as O2, which was used to distinguish the oxygen that connect with methyl to form an ester bond. The parameters of the bonds, angles and dihedrals of phosphate ester group have been provided in parmbsc0 in Amber14 that we needed not to fit again.

Table S6. The relationship between the inner diameter and the final minimized total energy of the 6HB. The lowest value is highlighted in red color.

Inner Diameter (Å)	Final Total Energy (kcal/mol)
18.0	$-2.4423*10^6$
18.2	$-2.4349*10^6$
18.4	$-2.4298*10^6$
18.6	$-2.4797*10^6$
18.8	$-2.4797*10^6$
19.0	$-2.5085*10^6$
19.2	$-2.5344*10^6$
19.4	$-2.5663*10^6$
19.6	$-2.5665*10^6$
19.8	$-2.5794*10^6$
20.0	$-2.5828*10^6$
20.2	$-2.5814*10^6$

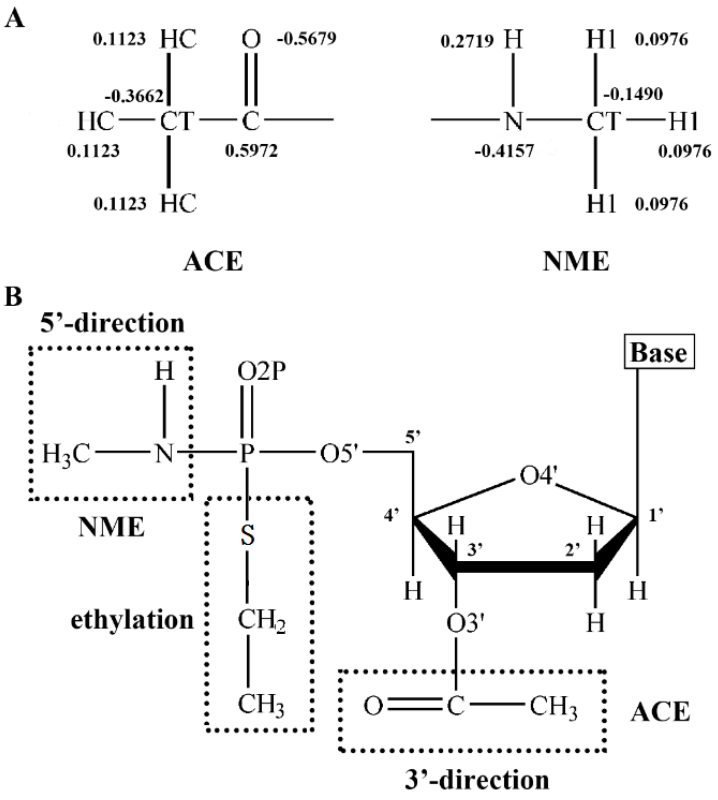

Figure S3. Structures of ACE, NME and ethyl-phosphorothioate DNA: A) Structures and charge distributions of the aminomethyl group (NME) and acetyl group (ACE). B) Structure of capped ethyl-phosphorothioate nucleic acid. The atom name of oxygen atom and phosphorus atom are given. NME in 5' direction, ACE in 3' direction and the ethyl-phosphorothioate group are illustrated in dashed box.

Table S7. The charge distribution of the ethyl-phosphorothioate nucleic acid.

DSX[a]	Atom Name	Atom Type	Charge
Phosphate	P	P	0.832224
	OP2	O2	-0.578947
	O5'	OS	-0.368555
Ethyl-thio	S'	S	-0.316967
	CS1	CT	0.057996
	HS11	HC	0.111441
	HS12	HC	0.111441
	CS2	CT	0.057996
	HS21	HC	0.053154
	HS22	HC	0.053154
	HS23	HC	0.053154
Sugar[b]	C5'	CT	-0.046631
	H5'1	H1	0.151207
	H5'2	H1	0.151207
	C4'	CT	-0.016457
	H4'	H1	0.160571
	O4'	OS	-0.294563
	C3'	CT	-0.154676
	H3'	H1	0.239153
	C2'	CT	-0.190147
	H2'1	HC	0.111441
	H2'2	HC	0.111441
	O3'	OS	-0.124360
	C1'	CT	-
	H1'	H2	-
Base[b]	-	-	-

[a] DSX is the modified ethyl-phosphorothioate nucleic acids, where X = A, T, C, G.

[b] The charge distributions of adenine, thymine, cytosine and guanine and C1' and H1' atom of sugar were derived from parm99 force field, not presented here.

MD simulation Methodology

We design MD simulations with two concentrations of Mg^{2+} and Na^{+} each. The AMBERff99 force fields with parambsc0 corrections, Na^{+} parameters of Joung/Cheatham and Mg^{2+} parameters of Li/Merz were used in our simulations. The details of five simulated systems were given in **Table S1**. It should be noted that ions concentration of our simulations were not equal to experiments. The reason is that in manning's theory,[9] no matter how dilute the solution, a number of the counterions remain in close proximity to the DNA, for Na^{+} counterions, It was 76% of DNA backbone negative charge. For Mg^{2+} counterions, it was 88%. In the condition of our systems' volume, to give the minimum monovalent counterions (total charge equal to zero) is 250 mM. To build a system with 100 mM Na^{+}, 12.5 mM Mg^{2+} or 50 mM Mg^{2+}, numbers of water molecule should be three to ten times above now. The total atom numbers of three systems need to be 1.5 million or 50 million, which is far above the GPU calculating tolerance. Moreover, far more time is need to equal the systems. Thus, we chose to simulate higher ion concentrations to investigate the relationship between 6HB's conformation and ions concentration.

Table S8. Details of the Simulated Systems

system	no. of atoms total	box dimension [x,y,z (nm)]	number of cations
NaL	549373	13,13,40	936
NaH	547586	13,13,40	1872
NaH_12E6HB	551212	13,13,40	1858
MgL	567159	13,13,40	468
MgH	506775	12,12,40	893
FullE6HB	535406	12,13,40	-

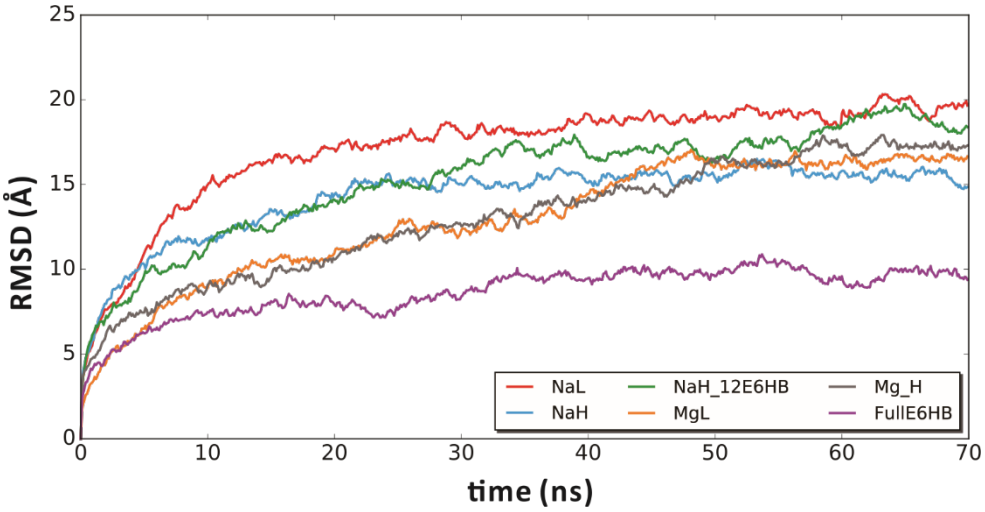

Figure S4. RMSD values of NaL (red), NaH (blue), NaH_12E6HB (green), MgL (orange), MgH (gray) and FullE6HB (magenta) during the 70 ns MD simulations.

Distance between helix

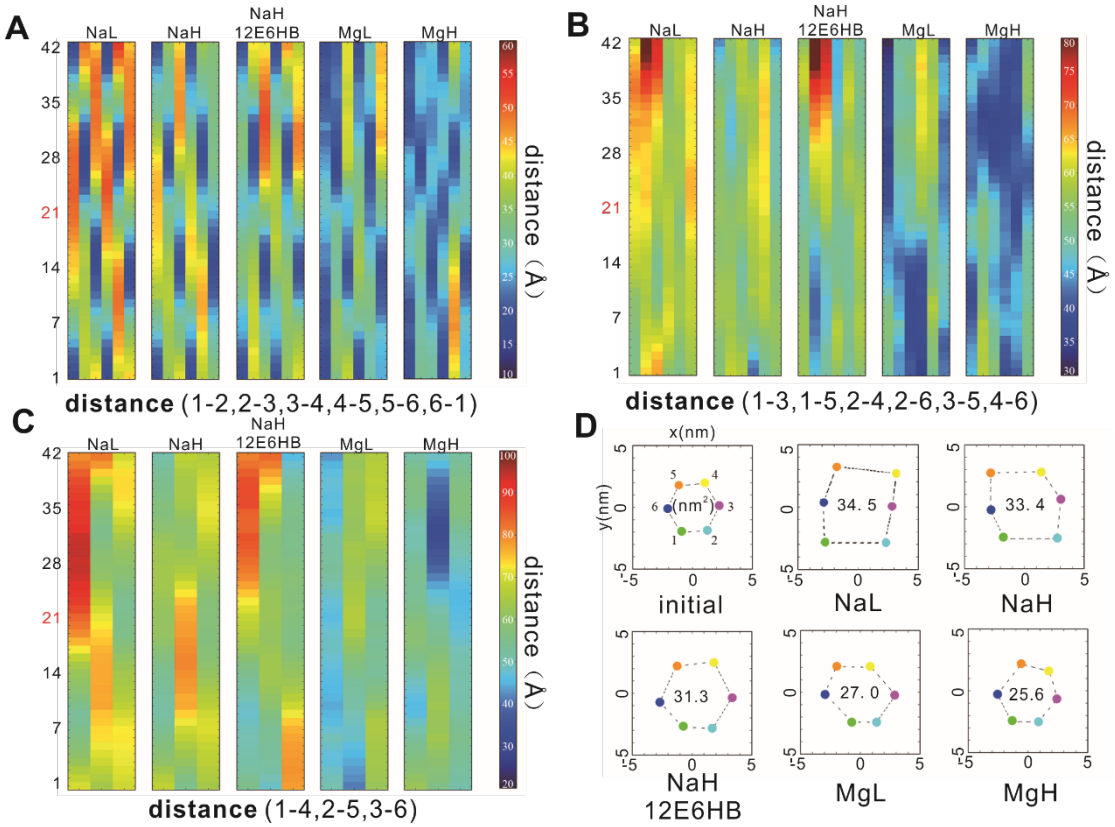

Figure S5. Distance between helix and section area of 6HB. A) Distance between ortho-position helix 1-2, 2-3, 3-4, 4-5, 5-6 and 6-1. B) Distance between meta-position helix. C) Distance between para-position helix. D) Section area of initial conformation and average conformation of last 5 ns of five system. In this plot, we can see the distance between helix shrink in order of NaL > NaH > NaH_12E6HB > MgL > MgH.

Radial pair distribution function of Na^+ and Mg^{2+} ions

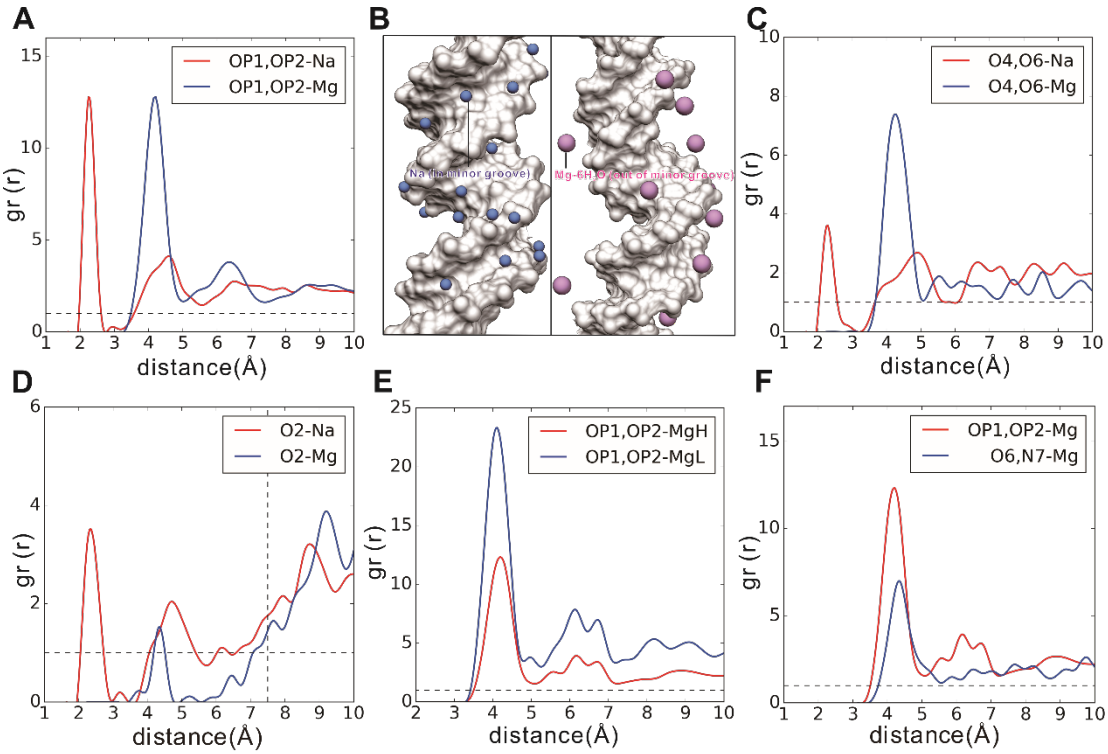

Figure S6. Na^+ and Mg^{2+} Ions distribution on DNA and Radial Pair Distribution Function g(r) of ions. To study the shape change of 6HB, in different ions conditions, we investigate the binding mode of Na^+ and Mg^{2+} with 6HB. From the MD simulation results, we found that: **A)** Na^+ ions prefers binding to phosphate directly (2.4 Å) where Mg^{2+} prefers binding with bridged water (4.4Å). **B)** Na^+ (blue) and Mg^{2+} (magenta) Ions distribution on B-DNA. **C)** Ions distribution in the major groove, we can see that the relative abundance ratio of Mg^{2+} is much greater than Na. **D)** Ions distribution in the minor groove, vertical black dotted line point out the boundary of intra and out minor groove. From this plot, we can observe that Na^+ can distribute in minor groove while Mg^{2+} cannot. This was because the stable water shell make Mg^{2+}-$6H_2O$ too big to get in the minor groove. **E)** Mg^{2+} distribution in MgL and MgH systems. In this plot, the abundance ratio of Mg^{2+} (250 mM) near OP1 or OP2 atom was almost two times of Mg^{2+} (500 mM). This result reveal that the Mg^{2+} ions near the phosphate group are nearly equally and the influence of different Mg^{2+} concentration (250/500 mM) on phosphate is slight. **F)** Distribution of Mg^{2+} on phosphate and major groove. Be compared to the major groove, Mg^{2+} prefers phosphate more.

The fully ethyl-phosphorothioate DNA

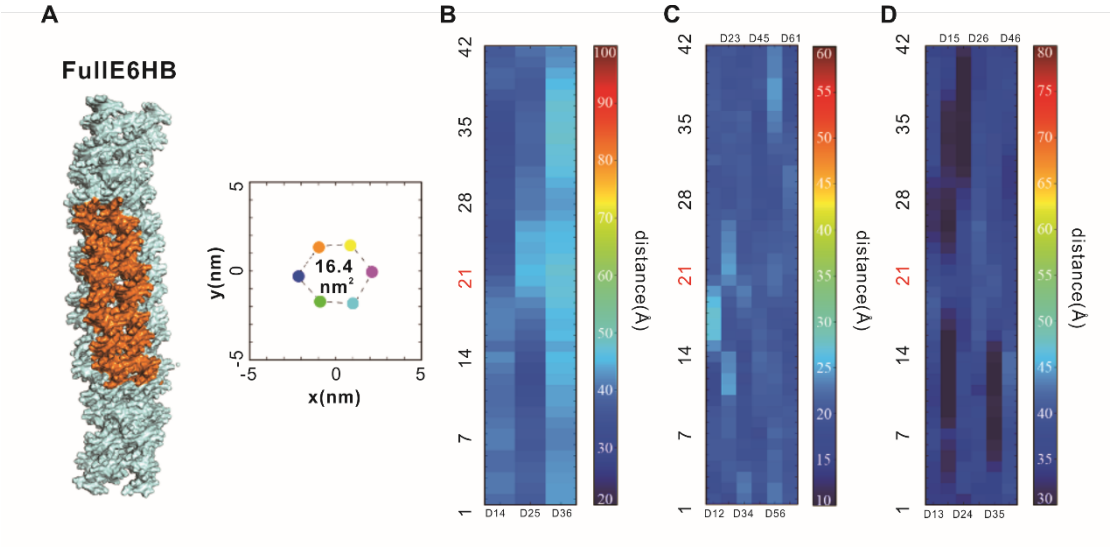

Figure S7. **Shape of fully ethyl-phosphorothioate DNA**. **A)** The average conformation of last 10 ns and, section area of FullE6HB. **B)** Distance between para-position. **C)** Distance between meta-position. **D)** Distance between othro-position.

Stretch module = 5336.82 ± 160.18 PN
Persistence length = 240.58 ± 15.48 nm

FULLE6HB show great increase in stretch module, which was caused by hydrophobic interaction of ethyl groups. On the other hand, compared to the 6HB in Na^+, the persistence length of FULLE6HB decrease a lot. We think the both the disappeared negative charge and reduced radius are response for this phenomenon.

Complementary pattern of 1-2, 4-5 helix distance of 12E6HB

In MD simulation system of NaH_12E6HB, the O-rings of helix1-2 and 4-5 were not always keep close both. However, **i**t can be seen that these two distances were complementary. **(Fig. S8)** We think that the tension of 12E6HB (**Fig. S9D**) is too strong for 8 modified base from holding both O ring. So when helix 12 was hold, the bridge of helix 45 would be broken, and vice versa.

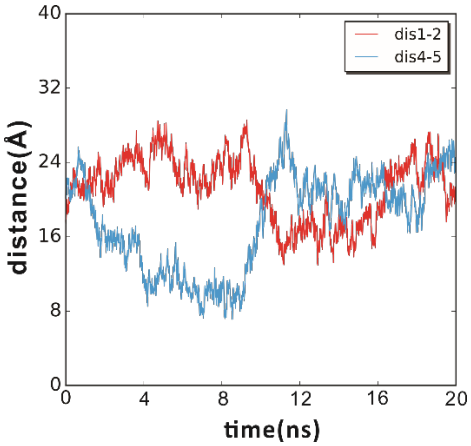

Figure S8. Complementary pattern of 1-2, 4-5 helix distance. The distance statistics between helix 12 and 45 was performed after the 50 ns.

Stretch modules and persistence length

Different from single helix, the rigidity of 6HB is decided by not only the rigidity of single helix but also the radius of 6HB and interaction between helix. In NaL and NaH systems, shrink radius of 6HB loose the tension on r direction, which give more space to 6HB to expand and shake on lengthwise direction (reducing on stretch modulus). Different from Na^+ systems, increasing concentration of Mg^{2+} deduced both length and radius of 6HB, which could be caused by the bridging interaction of Mg^{2+}-$6H_2O$ complex. Same as Mg^{2+} systems, in NaH_12E6HB system, restraint interaction bring by finger crossing of ethyl groups give 6HB an increasing on stretch modulus. In both ion systems, shrunk radius introduced decrease of persistence length. In addition, we calculated the stretch modulus and persistence length of FullE6HB. In this particularly system, all charge on backbone of 6HB was get rid of. As an consequence, more hydrophobic interaction between ethyl group bring increasing of stretch modulus, while reduced r bring deducing of persistence length **(Fig. S7, Fig. S9)**

In a canonical ensemble at constant temperature T, the probability of having an instantaneous contour length L can be given as:

$$\mathbf{P(L)} = \sqrt{\frac{\gamma \mathbf{L_0}}{2\pi \mathbf{k}_B \mathbf{T}}}\, e^{\frac{-\gamma \mathbf{L_0}}{2\pi \mathbf{k}_B \mathbf{T}}\left(\frac{L}{L_0}-1\right)^2} \qquad \textbf{eq. 1}$$

$$\mathbf{lnP(L)} = -\frac{\gamma L_0}{2k_B T}\left(\frac{L}{L_0}-1\right)^2 + C \qquad \textbf{eq. 2}$$

Where The L_0 is the average contour length, γ is the stretch modulus of the 6HBs

The probability of finding a small fluctuation θ in the bending angles of a flexible polymer in a canonical ensemble at temperature T can be written as:

$$\mathbf{P(\theta)} = \sqrt{\frac{\kappa}{2\pi \mathbf{k_B T L_0}}}\, e^{\frac{\kappa}{2\pi \mathbf{k_B T L_0}}\theta^2} \qquad \textbf{eq. 3}$$

$$\mathbf{lnP(\theta)} = -\frac{L_P}{L_0}(1 - cos\theta) + C \qquad \textbf{eq. 4}$$

Where κ is the bending modulus, k_B is the Boltzmann constant, and $L_p = \kappa/k_BT$ is the persistence length. The x3DNA[10] was used to analysis MD trajectory to fetch input data. The way to calculate stretch modulus and persistence length was as same as Garai's work[11].

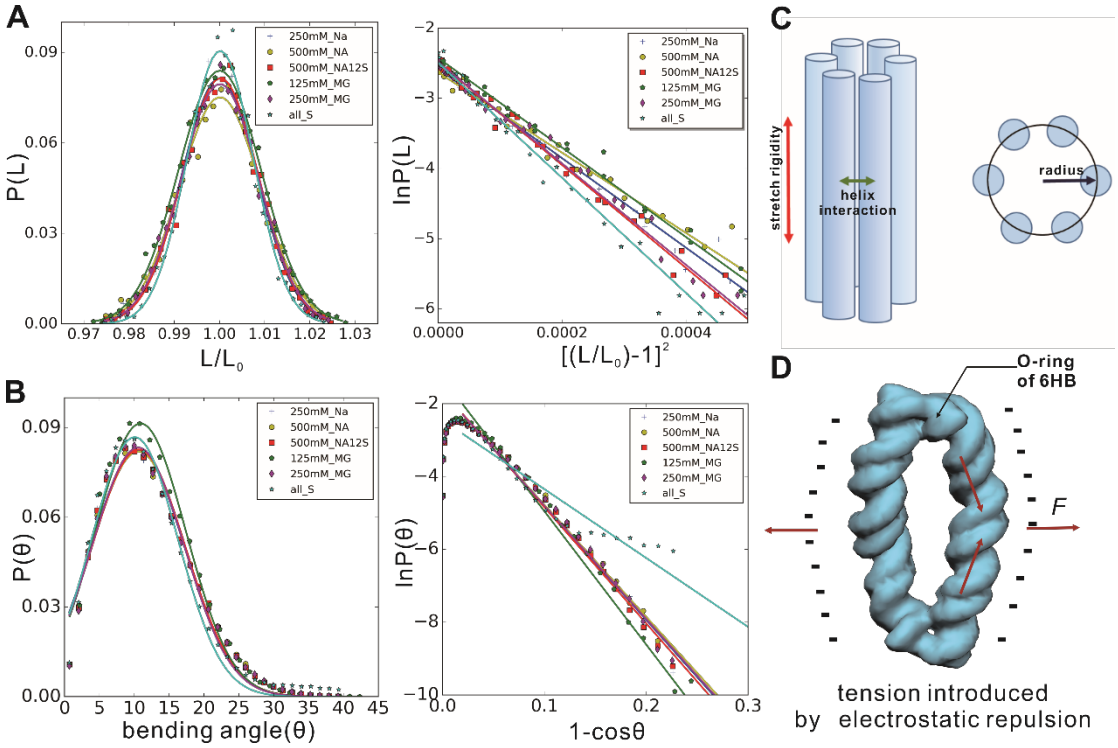

Figure S9. Mechanical property of 6HBs. A) Stretch modules calculation: contour length distributions of 6HBs in last 30 ns and semilog plot of P(L) vs $[(L/L_0) - 1]^2$. The solid line is fitting in eq1 and eq2. **B)** Persistence length calculation: bending angle distribution of the 6HBs and bending angle distribution as a function of 1 − cos(θ) in a semilog plot. The solid line is fitting in eq3 and eq4. **C)** Factors affect the mechanical property of 6HBs. **D)** In Na^+ systems, tension introduced by electrostatic repulsion may enhance stretch module.

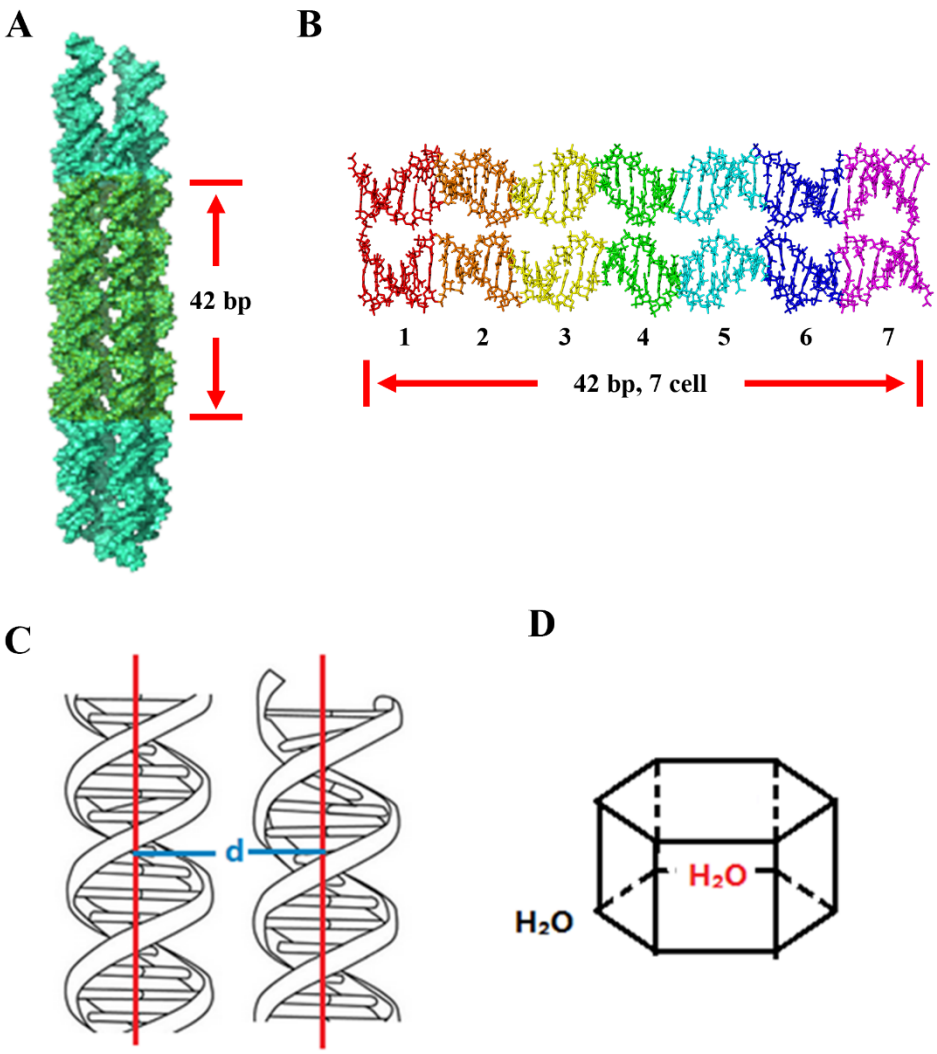

Figure S10. Definitions and calculation methods of nanostructural parameters. A) The relatively stable 42-bp region (grass green color). **B)** Further averagely segmented 7 cells in the 42-bp region. **C)** A motif of distance between two adjacent bundles. **D)** A motif of cavity for volume calculation. The waters in the hexagon column (colored red) were counted to calculate the cavity volume of nanotubes.

SAXS data fitting

SAXS was performed to validate the global reconfiguration of 6HB. The characteristic peak around q = 0.08 at low ion strength (100.0 mM Na^+) displays a distinct shift to lower-q region as ion strength increases (**Fig. S11d**), which indicates detectable structural change of 6HB. The combination of SAXS data and computational simulation can in principle yield accurate structures of biomolecules[12]. For this consideration, theoretical scattering profiles were calculated from atomic model of 6HB generated by MD and other modification methods (**Fig. S12-14**). Briefly, the fitting was achieved by initially performing NMA sampling on MD-generated models, and then structural energy minimization, followed by the evaluation via goodness-of-fit (denoted by χ^2) between theoretical and experimental scattering data, where each theoretical SAXS curve was calculated by Fast-SAXS-pro, which specially accounts for the hydration characteristic of DNA[4a]. The fitting results were also validated by Crysol and FoXS[4b, 13]. Note that a good agreement has been reached for the refined structures with the χ^2 value reduced from 156.8 to 18.5, 19.2 to 5.4 and 207.1 to 6.4, respectively, for 100 mM NaCl, 50 mM $MgCl_2$ and 125 mM $MgCl_2$ group (**Fig. S11e**). In addition, the root-mean-square deviation (RMSD) value for the initial MD-based and NMA-refined models were 1.384, 0.590 and 1.115 nm, respectively; the average diameters of three systems were: 6.75, 5.38 and 5.08 nm, which is quite close to the FRET experiment results (6.49, 5.32, 5.21 nm).

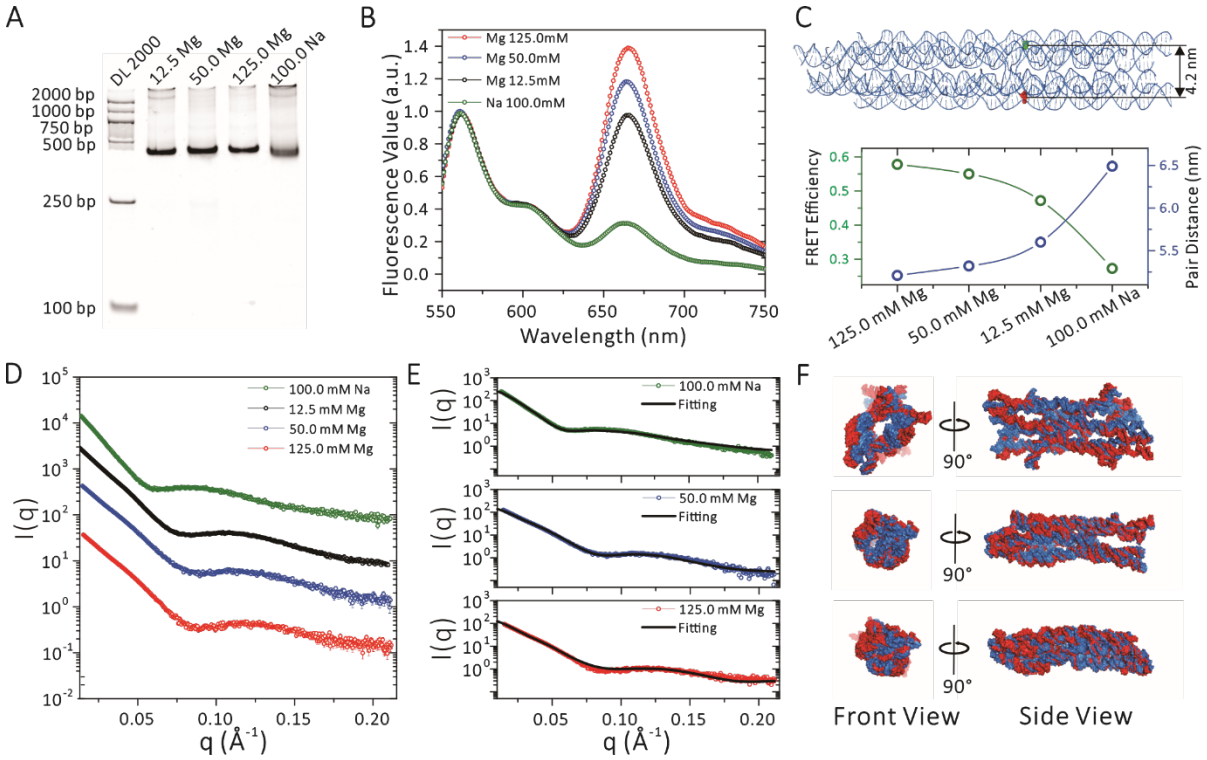

Figure S11. Experimental verification of the MD results for 6HB in different solutions. A) Non-denaturing gel electrophoresis of 6HB-DNA on native 6% polyacrylamide (PAGE) gel synthesized in different buffers. **B)** Normalized Förster resonance energy transfer (FRET) curves for samples with decreasing ion strength, which proves the increasing distance between Cy3 and Cy5 fluorescence pair. **C)** Schematic illustration of the FRET pair labelled on the 6HB DNA, trends of FRET efficiency and pair distance change. **D)** Small angle X-ray scattering (SAXS) intensities of four 6HB-DNA samples corresponding to FRET data. **E)** The optimized model fits based on Normal Mode Analysis (NMA) for 125.0 mM Mg, 50.0 mM Mg and 100.0 mM Na. **F)** Corresponding molecular models to SAXS profiles on the left side. Initial models obtained from MD are in blue, and the final models after refinements are in red, both front and side views are presented.

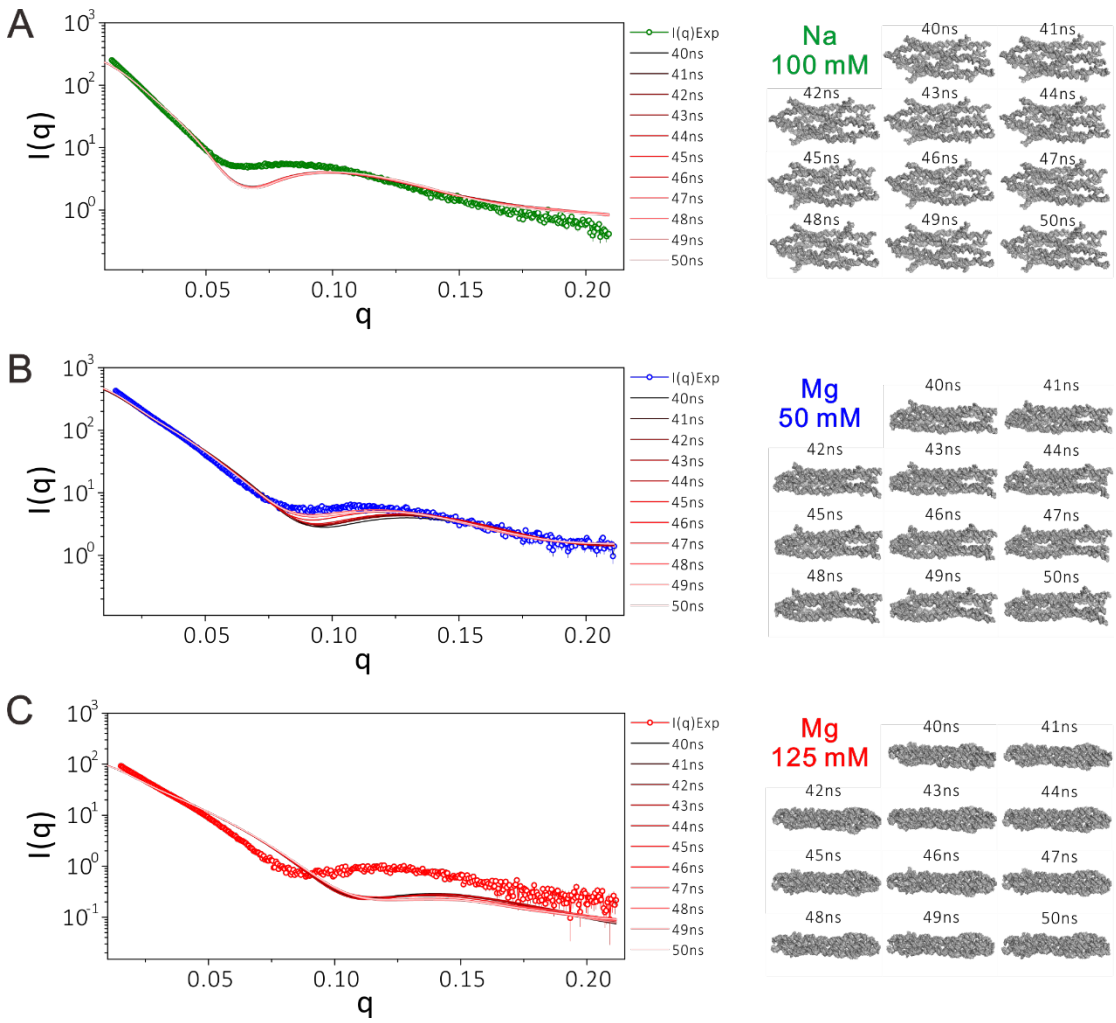

Figure S12. Direct fitting of experimental SAXS data using PDB models generated from MD simulation (Frames from 40 to 50 ns) in different solutions. A) 100 mM Na, **B)** 50 mM Mg, **C)** 125 mM Mg. From the fitting curve, one can point out that these MD-averaged conformation generally reproduced the overall shape of the experimental curves and characteristic peaks. However, all of the fitting curves of each group slightly red shifted from the experimental results. Which means the simulated structures are more compact than practical situation. Out of which, the 50 mM Mg group has the lowest mean χ^2 value (Given by Crysol) around 19.2, while for 100 mM Na and 125 mM Mg, the mean χ^2 value are around 156.8 and 207.1, respectively. The possible reason is due to the imperfection of force fields. Therefore, the following model adjustments are necessary.

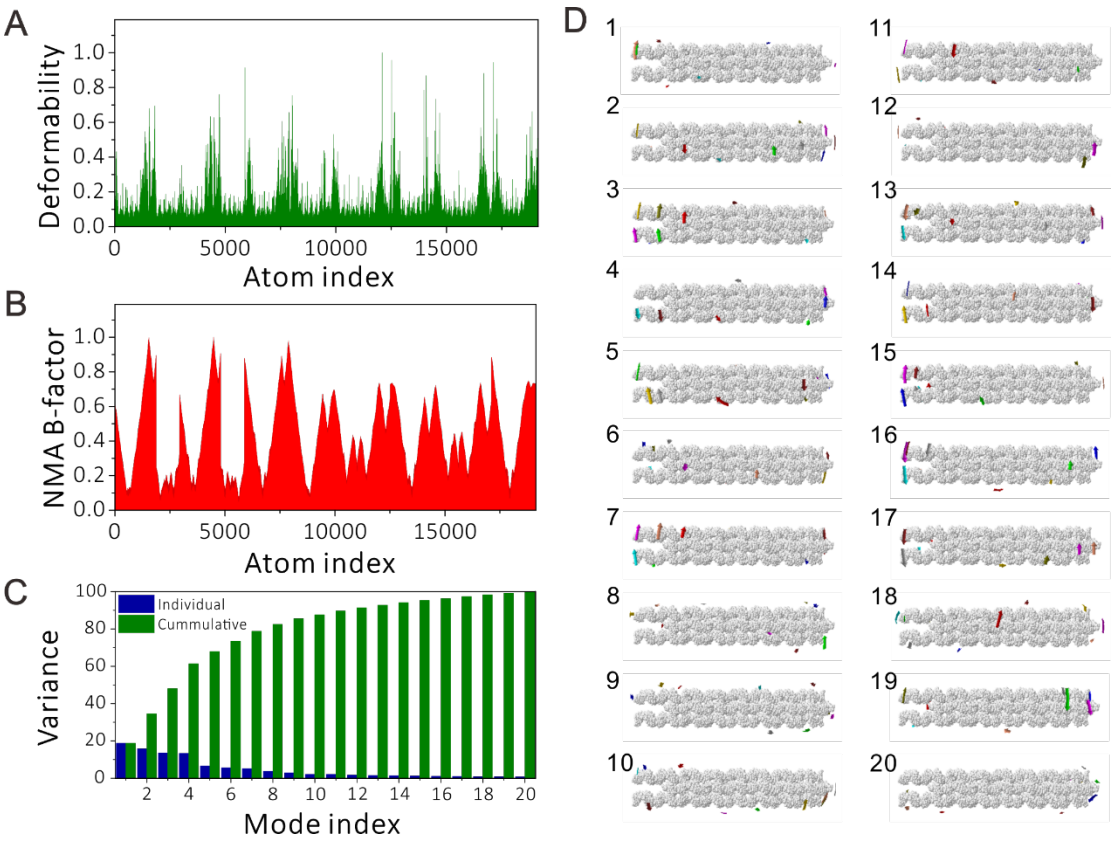

Figure S13. Structural information of ideal 6HB PDB models and representative NMA motion modes given by iMods online sever (iMOD.chaconlab.org). A, B) Structure mobility and B-factor. The mobility of 6HB at each of its residues was described by main-chain deformability. According to the DNA sequence design of 6HB, there existed several positions with high mobility, which have deformability values over 0.4. The NMA B-factor is calculated by multiplying the NMA mobility by $8\pi^2$. **C)** iMods provided 20 normal modes, the energy required to deform the structure is directly related to eigenvalue of each modes. The variance is inversely related to eigenvalue. The blue bars indicated individual variance of each mode, and green bars indicated the accumulated variances, which pointed out the first 5 modes will generate about 70% deformation of 6HB structure and the rest modes will produce slightly change. **D)** Schematic illustration plotted by JSmol of 20 normal modes. The colored affine arrows represented the force field applied on 6HB structure.

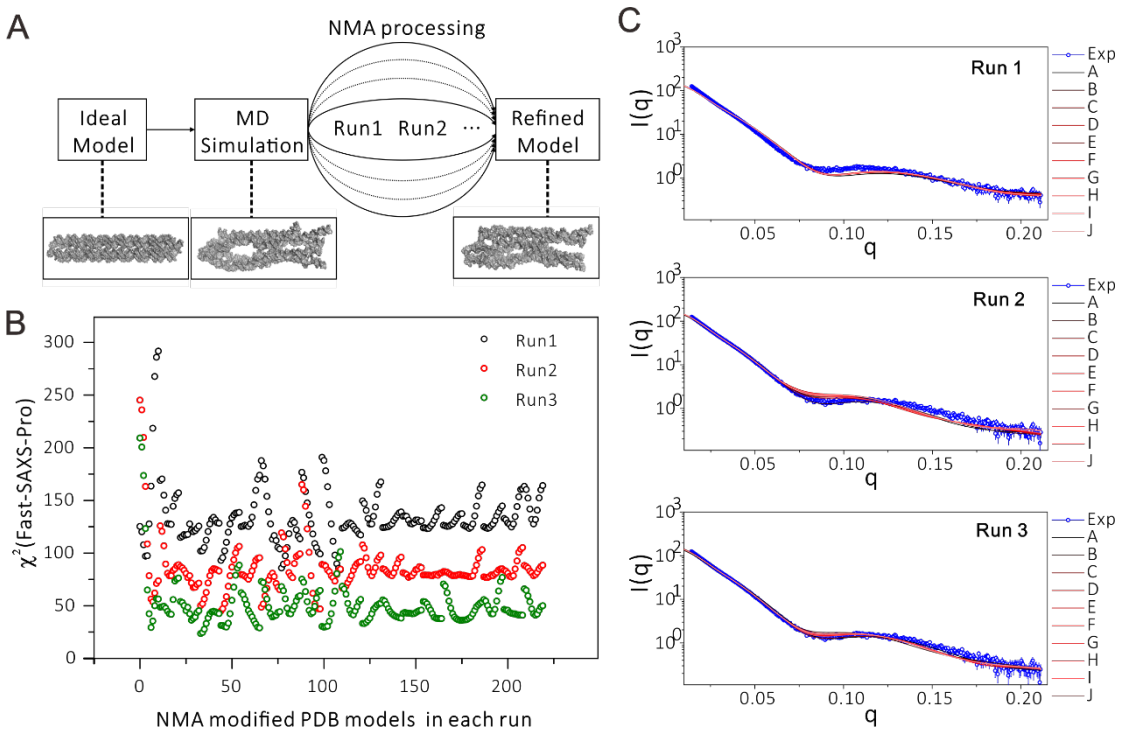

Figure S14. A typical model refine process using 50 mM Mg group as sample. A) Schematic illustration of model refinements. The ideal 6HB model was first applied a 50 ns MD simulation with corresponding ion environment, the model with lowest χ^2 value was then flowed by NMA processing with appropriate amplitude values (1.0 to 5.0, a greater amplitude value will generate larger deformation and reduce total calculation time, meanwhile, the structure will be more likely to collapse). If the previous fitting of PDB model set didn't produce a well enough χ^2 value, the model has a calculated SAXS curve that was most close to experimental data will be put into the next turn of NMA processing, namely, run 1, run 2, and so on. The χ^2 value will finally reach a minimum value after enough running turns. But in practical, the final results will consider time consuming and SAXS fitting factor simultaneously. **B)** The summarized χ^2 values (Given by Fast-SAXS-pro) of first three run for 50 mM Mg sample. **C)** Corresponding fitting curves for the best ten models in each run.

Characterization and purification of ethylized DNA

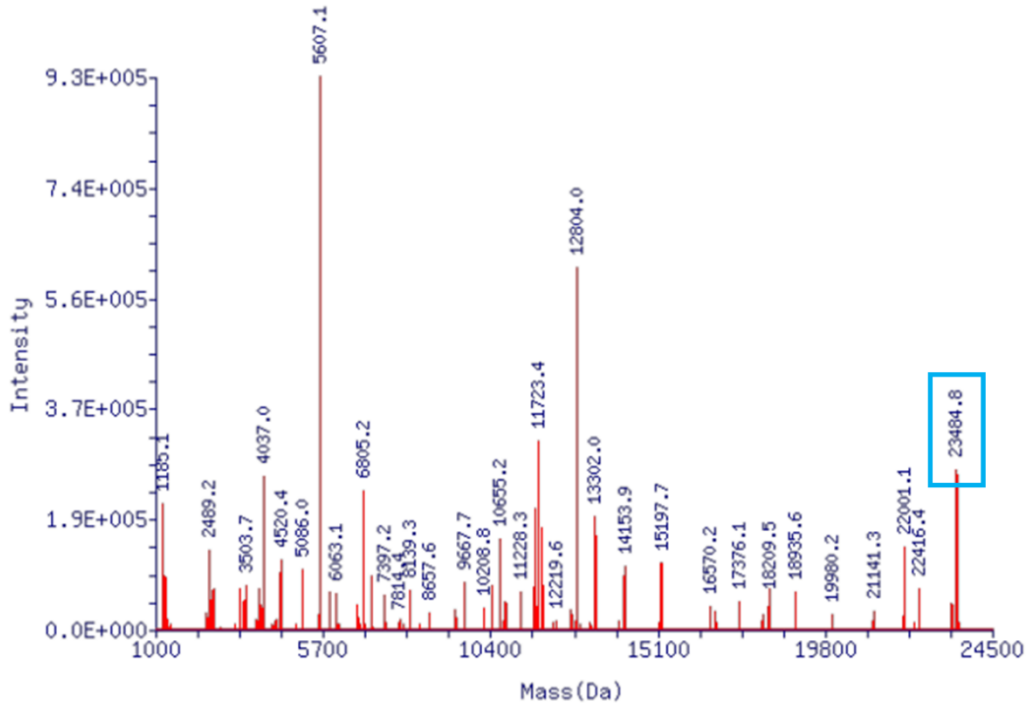

Figure S15. Mass Spectra of ssDNA chain No. A after ethylation. Before ethylation, the theoretical molecule weight of this ssDNA chain is 23434.2. The MS results proved a total molecule weight of 23484.8, with an increase of 50.6, slightly smaller than theoretical value of 58.0. Which indicated the success of ethylation.

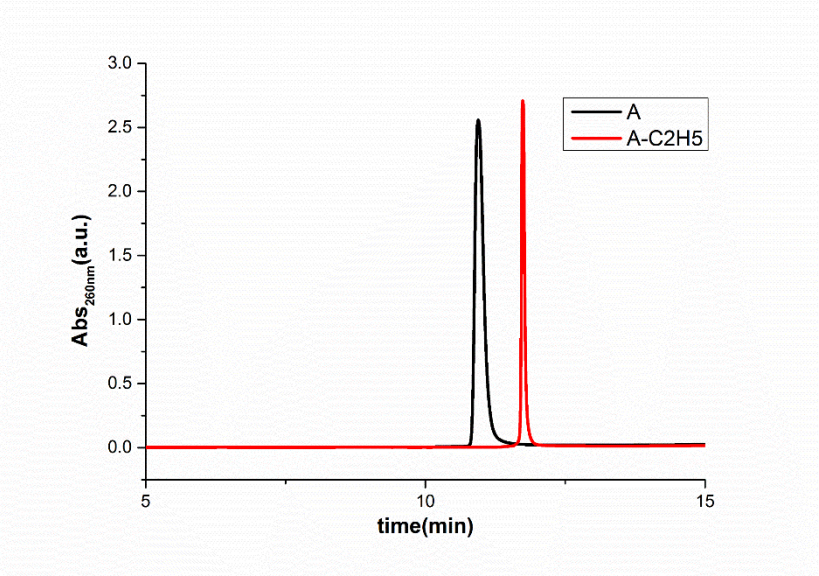

Figure S16. RP-HPLC elution profile for chain A before and after ethylation. The detailed RP-HPLC methods are as following.

Table S9. HPLC Protocol

Methods	Time（min）	%A	%B
a		98	2
b	10	70	30
c	25	2	98
d	26	98	2
e	36	98	2

Elution buffer A: 0.1M Triethyl ammonium bicarbonate,
Elution buffer B: acetonitrile, Flow rate: 0.8mL/min.

The DNA fraction was purified by RP-HPLC using a Waters system with a Waters 1525 pump and a Waters 2998 detector. The purification was performed using a Waters C18 column (150 x 4.6 mm, 5 µm beads, flow rate of 0.8 mL/min) using the following gradient: at 0 min 98% triethyl ammonium bicarbonate buffer (TEAB) pH 8.0 / 2% acetonitrile (ACN), from 0.1 to 10 min, 70% TEAB/ 30% ACN; from 10.1 to 25 min, 2% TEAB/ 98% ACN; from 25 to 26 min, 98% TEAB/ 2% ACN; and continued to 36 min.

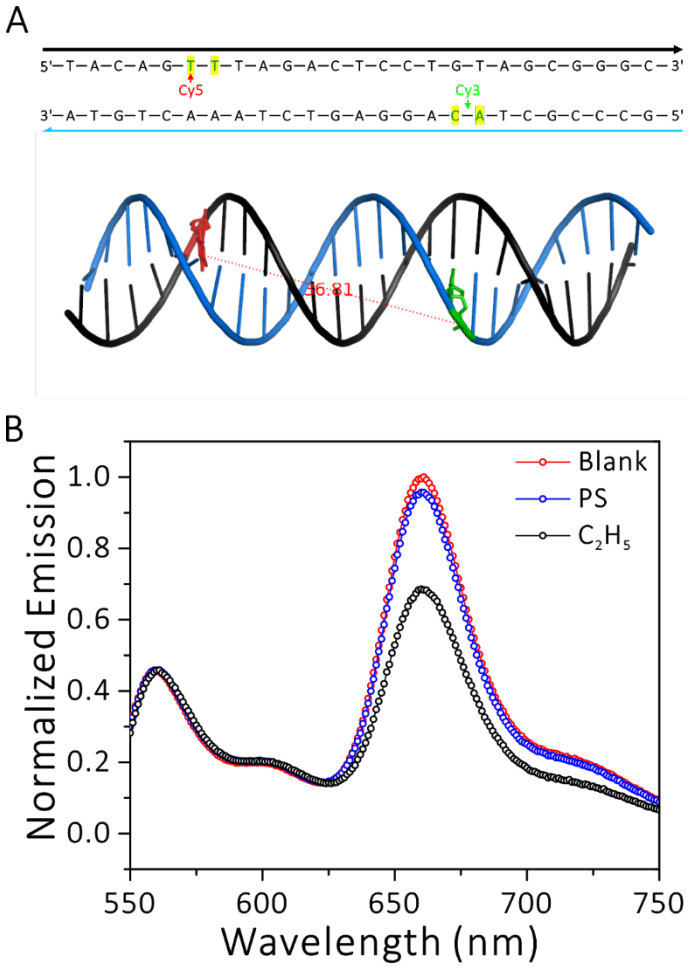

Figure S17. Influence of ethylation on Förster resonance energy transfer (FRET) efficiency. A) Design of 25 base pairs long dsDNA, the labeling sites of Cy3 and Cy5 are pointed out by arrow head. Two ethylized DNA bases on each chain are highlighted by yellow background. The ideal distance between the FRET pair is about 3.7 nm. **B)** FRET curves for unmodified dsDNA (Blank), phosphorothioate-dsDNA (PS), and ethylized dsDNA (C_2H_5). The results prove that both phosphorothiolation and ethylation will reduce FRET efficiency, while the effect of ethylation is much higher. This phenomenon made FRET based distance calculation inapplicable for ethylized DNA, because the reducing of FRET efficiency is not completely result from FRET pair distance variation.

Term list

Abbreviation	Full name	Comments
NMA	Normal Mode Analysis	A coarse-grained elastic network model that has been applied to deform macromolecular structures, such as protein and DNA, to fit and refine experimental data.
RMSD	Root-mean-square deviation	A measure of the differences between two structure conformations $\mathrm{RMSD} = \sqrt{\frac{\sum_{i=1}^{n}((X_i - X)^2 + (Y_i - Y)^2 + (Z_i - Z)^2)}{n}} \ldots\ldots \mathbf{eq.\ 5}$
g(r)	Radial distribution function	g(r) in a system of particles (atoms, molecules, colloids, etc.), describes how density varies as a function of distance from a reference particle.
PDB	Protein Data Bank	A crystallographic database for 3D structural data of large biological molecules, such as nucleic acids and proteins.
Rg	Radius of gyration	The root mean square distance of the object's parts from either its center of mass or a given axis. Especially, in SAXS study, Rg is used to describe the geometrical dimensions of a given particle, e.g., sphere, cylinder, and plate.
vdW	Van der Waals force	The nonbonded interaction comprises electrostatic force and Van der Waals force (as in **eq. 6**). When negative charges on DNA backbone present, the repulsive electrostatic force is much stronger than vdW force and dominates the nonbonded interaction. While with ethyl-phosphorothioate, the electrostatic repulse interaction was weakened and vdW interaction dominates. $E_{nonbonded} = E_{electrostatic} + E_{Van\ der\ Waals} = \sum_{j=1}^{N-1}\sum_{i=j+1}^{N} f_{ij}\left\{\frac{q_i q_j}{4\pi\varepsilon_0 r_{ij}} + \varepsilon_{ij}\left[\left(\frac{r_{0ij}}{r_{ij}}\right)^{12} - 2\left(\frac{r_{0ij}}{r_{ij}}\right)^{6}\right]\right\} \ldots \mathbf{eq.\ 6}$

Reference

[1] aI. G. Gut, S. Beck, *Nucleic Acids Res.* **1995**, *23*, 1367-1373; bJ. R. Burns, N. Aljuffali, S. M. Janes, S. Howorka, *Angew. Chem. Int. Ed.* **2014**, *53*, 12466-12470.

[2] aA. A. Deniz, M. Dahan, J. R. Grunwell, T. Ha, A. E. Faulhaber, D. S. Chemla, S. Weiss, P. G. Schultz, *Proc. Natl Acad. Sci. USA* **1999**, *96*, 3670-3675; bT. Heyduk, *Curr. Opin. Biotech.* **2002**, *13*, 292-296.

[3] S. S. Nielsen, K. N. Toft, D. Snakenborg, M. G. Jeppesen, J. K. Jacobsen, B. Vestergaard, J. P. Kutter, L. Arleth, *J. Appl. Crystallogr.* **2009**, *42*, 959–964.

[4] aK. M. Ravikumar, W. Huang, S. Yang, *J. Chem. Phys.* **2013**, *138*, 024112; bM. V. Petoukhov, D. Franke, A. V. Shkumatov, G. Tria, A. G. Kikhney, M. Gajda, C. Gorba, H. D. T. Mertens, P. V. Konarev, D. I. Svergun, *J. Appl. Crystallogr.* **2012**, *45*, 342–350.

[5] F. Mathieu, S. Liao, J. Kopatsch, T. Wang, C. Mao, N. C. Seeman, *Nano Lett.* **2005**, *5*, 661-665.

[6] W. D. Cornell, P. Cieplak, C. I. Bayly, I. R. Gould, K. M. Merz, D. M. Ferguson, D. C. Spellmeyer, T. Fox, J. W. Caldwell, P. A. Kollman, *J. Am. Chem. Soc.* **2015**, *117*, 5179-5197.

[7] A. Pérez, I. Marchán, D. Svozil, J. Sponer, C. A. Laughton, M. Orozco, *Biophys. J.* **2007**, *92*, 3817-3829.

[8] W. D. Cornell, P. Cieplak, C. I. Bayly, P. A. Kollmann, *J. Am. Chem. Soc.* **1993**, *115*, 9620-9631.

[9] aG. S. Manning, *Ber. Bunsenges. Phys. Chem.* **1996**, *100*, 909-922; bG. S. Manning, *Macromolecules* **2001**, *34*, 4650-4655.

[10] A. V. Colasanti, X. J. Lu, W. K. Olson, *Jove-J. Vis. Exp.* **2011**, *74*, e4401.

[11] A. Garai, S. Saurabh, Y. Lansac, P. K. Maiti, *J. Phys. Chem. B* **2015**, *119*, 11146-11156.

[12] S. Yang, *Adv. Mater.* **2014**, *26*, 7902-7910.

[13] aD. Schneidman-Duhovny, M. Hammel, J. A. Tainer, A. Sali, *Nucleic Acids Res.* **2016**, *44*, W424-W429; bD. Schneidmanduhovny, M. Hammel, J. A. Tainer, A. Sali, *Biophys. J.* **2013**, *105*, 962-974.